Particle-Based Methods for Mesoscopic Transport Processes

106

Zhen Li, Wenxiao Pan, and Alexandre M. Tartakovsky

Contents

Abstract

Biological phenomena at cellular and subcellular levels involve transport of reacting biochemical species, including proteins, enzymes, and nutrients. At the mesoscopic scale, stochastic effects can play an important role and dominate the biological processes. Therefore, the continuum deterministic description, which ignores fluctuations, becomes no longer accurate. To this end, mesoscopic methods with stochastic terms are attracting more attention as a promising approach for tackling challenging problems in cellular biology and bioengineering. This chapter describes particle-based stochastic models for mesoscopic transport processes, including thermal transport, reactive chemical transport, and ionic transport in mesoscopic systems.

Z. Li (✉)
Department of Mechanical Engineering, Clemson University, Clemson, SC, USA
e-mail: zli7@clemson.edu

W. Pan
Department of Mechanical Engineering, University of Wisconsin-Madison, Madison, WI, USA
e-mail: wpan9@wisc.edu

A. M. Tartakovsky
Computational Mathematics Group, Pacific Northwest National Laboratory, Richland, WA, USA
e-mail: alexandre.tartakovsky@pnnl.gov

W. Andreoni, S. Yip (eds.), *Handbook of Materials Modeling*,
https://doi.org/10.1007/978-3-319-44680-6_64

1 Introduction

At the mesoscopic scale, thermal fluctuations and discrete features play important roles in biological processes, and the classical approaches based on deterministic transport equations are inadequate to predict the time evolution of the mesoscale biological system (Hellander 2008). Deterministic equations are formulated as a system of (generally, nonlinear) ordinary differential equations (ODEs) and partial differential equations (PDEs) for the dynamics of mean-field concentrations of the biochemical species. However, at cellular and subcellular levels, the biological processes present considerable variations from cell to cell (Chen et al. 2017). The variations arise from the fact that the cells are so small that the discrete features and stochastic effects become crucial and may play a significant role in the relevant dynamics. Therefore, to accurately model biological processes at the mesoscopic scale, a better approach involves developing discrete particle-based methods suitable for stochastic processes, where the discreteness of the biochemical species and the randomness of transports and reactions are explicitly accounted for. From a modeling point of view, stochastic dynamics is considerably harder to simulate and analyze than the mean-field behavior (Schnoerr et al. 2017).

For mesoscopic processes driven by thermal noises, a popular approach that accounts for the effects of thermal fluctuations is the Markovian stochastic process, where stochastic terms induced by equilibrium or non-equilibrium fluctuations can be modeled in terms of Gaussian white noise (Ortiz de Zárate and Sengers 2006). A Markovian approximation is valid when the correlation time of fluctuations is much shorter than the characteristic timescale of the dynamics of fluid particles/voxels. This is true as long as the size of fluid particles/voxels is much larger than the biochemical molecule size. As the size of fluid particle/voxel becomes comparable with the molecule size, it is anticipated that the macroscopic or mesoscopic modeling framework based on equilibrium/non-equilibrium statistics will fail to describe the underlying system dynamics accurately. In this regard, microscale methods with much higher computational cost, such as the reaction-diffusion master equation (RDME) (Drawert et al. 2016; Schnoerr et al. 2017), must be employed to attain insight into the discrete features of biochemical reactive transport.

This chapter focuses on recent advances in particle-based methods, including dissipative particle dynamics (DPD), smoothed particle hydrodynamics (SPH), and smoothed dissipative particle dynamics (SDPD), for mesoscale transport processes. In these methods, the stochastic terms induced by thermal fluctuations are modeled as Markov processes. Developing these methods has provided not only a deeper understanding of the transport processes in the presence of fluctuations but also a framework for modeling non-equilibrium processes of mesoscopic systems using a local equilibrium approximation and investigating the energetic fluctuations of mesoscopic transport in biological systems and beyond. Methods for thermal transport at the mesoscopic scale are introduced in Sect. 2. The methods for modeling mesoscopic reactive transport are discussed in Sect. 3. Section 4 presents the methods for modeling mesoscopic ionic transport, and Sect. 5 concludes with a brief summary and discussion.

2 Mesoscopic Thermal Transport

Compared to healthy tissues, unhealthy tissues (especially tumors and cancers) usually have lower pH values and higher temperatures stemming from microenvironment abnormalities (Taghizadeh et al. 2015). The differences between unhealthy and healthy tissues can be used to design targeted therapies. For example, based on the fact that tumor microenvironments are slightly hyperthermic, thermosensitive polymers and liposomes can be used as targeted drug carriers to effectively deliver drugs to tumor cells without harming healthy cells (Perez-Herrero and Fernandez-Medarde 2015). However, developing thermosensitive drug delivery techniques with controllable drug release in non-isothermal processes requires a fundamental understanding of the mesoscopic thermal transport and knowledge of the role thermal fluctuations play in biological processes. This section introduces two mesoscopic modeling methods that can provide such fundamental understanding and knowledge.

First, Avalos and Mackie (1997) and Español (1997) developed an energy-conserving DPD (eDPD) model that augments the classical DPD model with the internal energy as an additional property of each DPD particle. The classical DPD model was developed based on equilibrium thermodynamics (Español and Warren 1995), where the dissipative and random forces satisfying the fluctuation-dissipation theorem act as a thermostat to maintain the system at a constant temperature. Thus, the classical DPD method is limited to modeling isothermal systems and can neither sustain temperature gradients nor model thermal transport in non-isothermal processes (Li et al. 2017). In contrast, in the eDPD method, each eDPD particle is considered as a coarse-grained particle associated with an internal energy in addition to other quantities, such as position and momentum. The stochastic differential equations governing the dynamics of eDPD particles include the conservations of momentum and energy in the form of (Li et al. 2014):

$$
\begin{aligned}
m_i \frac{\mathrm{d}^2 \mathbf{r}_i}{\mathrm{d}t^2} &= m_i \frac{\mathrm{d}\mathbf{v}_i}{\mathrm{d}t} = \mathbf{F}_i = \sum_{i \neq j} (\mathbf{F}_{ij}^C + \mathbf{F}_{ij}^D + \mathbf{F}_{ij}^R) \; , \\
C_v \frac{\mathrm{d}T_i}{\mathrm{d}t} &= q_i = \sum_{i \neq j} (q_{ij}^C + q_{ij}^V + q_{ij}^R) \; ,
\end{aligned}
\tag{1}
$$

where m, t, $\mathbf{r}_i$, $\mathbf{v}_i$, and $\mathbf{F}_i$ denote mass, time, position, velocity, and force vectors, respectively. T_i represents the temperature, C_v the thermal capacity, and q_i the net heat flux of particle i. The summations of force and heat flux are carried out over all particles within a cutoff radius r_{cf} from particle i for forces and a cutoff radius r_{ct} for heat fluxes.

The three components of $\mathbf{F}_i$, including conservative, dissipative, and random forces, are given by $\mathbf{F}_{ij}^C = a_{ij} w_C(r_{ij}) \mathbf{e}_{ij}$, $\mathbf{F}_{ij}^D = -\gamma_{ij} w_D(r_{ij})(\mathbf{e}_{ij} \cdot \mathbf{v}_{ij})\mathbf{e}_{ij}$, and $\mathbf{F}_{ij}^R \mathrm{d}t = \sigma_{ij} w_R(r_{ij}) \mathrm{d}W_{ij} \mathbf{e}_{ij}$, respectively (Groot and Warren 1997). The coefficients a, γ, and σ determine the strength of each force. The weight functions $w_C(r)$,

$w_D(r)$, and $w_R(r)$ are defined with a cutoff radius r_{cf} beyond which these weight functions vanish. $\mathrm{d}W_{ij} = \mathrm{d}W_{ji}$ are independent increments of the Wiener process. Using the assumption of local thermodynamic equilibrium, Español (1997) derived a Fokker-Planck equation (FPE) for the stochastic equation (1). The FPE solution gives the relationship between the dissipative force and the random force, which requires $\sigma_{ij}^2 = 4\gamma_{ij}k_B T_i T_j/(T_i + T_j)$ and $w_D(r) = w_R^2(r)$. It indicates that the fluctuation-dissipation theorem is applied locally based on the particle temperature T_i instead of the system's thermodynamic temperature, stressing the local nature of the eDPD model (Avalos and Mackie 1997). The heat fluxes between two particles i and j, accounting for the thermal conduction q_{ij}^C, viscous heating q_{ij}^V, and random heat flux q_{ij}^R, are given by (Li et al. 2014)

$$q_{ij}^C = k_{ij} w_{CT}(r_{ij}) \left(T_i^{-1} - T_j^{-1}\right) , \tag{2a}$$

$$q_{ij}^V = \frac{1}{2C_v}\left\{ w_D(r_{ij}) \left[\gamma_{ij} \left(\mathbf{e}_{ij}\cdot\mathbf{v}_{ij}\right)^2 - m_i^{-1}\sigma_{ij}^2\right] - \sigma_{ij} w_R(r_{ij}) \left(\mathbf{e}_{ij}\cdot\mathbf{v}_{ij}\right)\xi_{ij}\right\} , \tag{2b}$$

$$q_{ij}^R = \beta_{ij} w_{RT}(r_{ij})\xi_{ij}^e , \tag{2c}$$

where the thermal conduction q_{ij}^C contains T^{-1} rather than T because the thermodynamic quantity conjugated to the internal energy is the inverse of the temperature instead of the temperature itself (Español 1997). The parameters k_{ij} and β_{ij} determine the strength of the thermal conduction and the random heat flux, respectively. In particular, k_{ij} plays the role of a thermal conductivity given as $k_{ij} = C_v^2\kappa(T_i + T_j)^2/4k_B$, where κ is interpreted as a mesoscale heat friction coefficient. The relationships $\beta_{ij}^2 = 2k_B k_{ij}$ and $w_{CT}(r) = w_{RT}^2(r)$ are required to satisfy the fluctuation-dissipation theorem. A common choice of the weight functions is $w_{CT}(r) = w_{RT}^2(r) = (1 - r/r_{\mathrm{ct}})^{s_T}$ with a cutoff radius r_{ct}, where the case of $s_T = 2.0$ corresponds to the typical quadratic weighting function (Groot and Warren 1997).

For an eDPD particle, the characteristic scale of the kinetic energy related to its momentum is $k_B T$, while the characteristic scale of the internal energy related to its temperature is $C_v T$. A scaling factor $k_B T/C_v T$ is required to convert kinetic energy into internal energy. Therefore, the heat flux q_{ij}^V due to viscous heating given by Eq. (2b) has a factor $1/C_v$ when the kinetic energy $k_B T$ is taken as the energy unit. Also, the factor 2 in the denominator guarantees that the heat generated by nonconservative interactions is distributed evenly to both particles of a pair. Through numerical experimentation, Li et al. (2014) demonstrated that Eqs. (1) and (2) conserve energy.

The transport properties, such as diffusivity and viscosity, do not need to be prescribed in eDPD. Groot and Warren (1997) and Marsh et al. (1997) have derived the expressions of diffusivity and kinematic viscosity in terms of DPD parameters, which are given as

$$D = \frac{3k_BT}{4\pi\gamma\rho}\left(\int_0^\infty r^2 g(r) w_D(r) dr\right)^{-1}, \quad \nu = \frac{D}{2} + \frac{2\pi\gamma\rho}{15}\int_0^\infty r^4 g(r) w_D(r) dr, \tag{3}$$

where $g(r)$ is the radial distribution function. A rough analytical prediction of D and ν can be obtained by substituting $w_D(r) = w_R^2(r) = (1 - r/r_{\mathrm{cf}})^s$ and $g(r) = 1.0$ into Eq. (3), which leads to $D = 3k_BT\prod_{i=1}^{3}(s+i)/8\pi\gamma\rho r_{\mathrm{cf}}^3$ and $\nu = D/2 + 16\pi\gamma\rho r_{\mathrm{cf}}^5/5\prod_{i=1}^{5}(s+i)$.

The DPD fluid's thermal conductivity also can be calculated in terms of the model parameters. When the energy transport is dominated by thermal conduction, the macroscopic thermal conductivity λ can be calculated as (Mackie et al. 1999)

$$\lambda = \frac{2\pi}{3}\frac{\rho^2}{T^2}\int_0^\infty r^4 k w_{CT}(r) g(r) dr \ , \tag{4}$$

where $k = C_v^2\kappa T^2/k_B$ and $w_{CT}(r)$ is the weight function. Given $w_{CT}(r) = (1 - r/r_{\mathrm{ct}})^{s_T}$ and $g(r) = 1.0$, an analytical estimate for the thermal conductivity λ can be obtained as $\lambda = 16\pi\rho^2\kappa C_v^2 r_{\mathrm{ct}}^5/k_B\prod_{i=1}^{5}(s_T+i)$. In particular, when the typical quadratic weight function $(1 - r/r_{\mathrm{ct}})^2$ is adopted for $w_{CT}(r)$, $\lambda = 2\pi\rho^2\kappa C_v^2 r_{\mathrm{ct}}^5/315k_B$. Let $\mathrm{Pr} = \rho\nu C_v/\lambda$ be the Prandtl number, which is a dimensionless number whose value can be obtained from experiments. By replacing λ with Pr, the result is a formula for determining the mesoscale heat friction κ given by $\kappa = 315k_B\nu/2\pi\rho\mathrm{Pr}C_v r_{\mathrm{ct}}^5$. Notably, this formula is obtained from the typical quadratic weight function. When a different weight function is employed, a similar formula could be derived from Eq. (4).

The expression of Eq. (3) indicates that both the diffusivity D and kinematic viscosity ν of the eDPD fluid increase linearly with the temperature if other variables in Eq. (3) remain constant. However, for most of the liquids, including water, ethanol, and glycerin, the diffusivity increases, but the kinematic viscosity decreases with increasing temperature. To correct the temperature-dependent properties (diffusivity, viscosity, and thermal conductivity) of these liquids, Li et al. (2014) analyzed the sensitivity of D, ν, and λ with respect to the model parameters and defined the exponent of the weighting function s as a function of temperature. They took liquid water as an example and demonstrated that the eDPD model can produce the correct temperature-dependent diffusivity and viscosity, as well as Prandtl numbers, for various temperatures, which is consistent with available experimental data. For details on the eDPD model parameterization, refer to Li et al. (2014) and Lei et al. (2017).

Alternatively to the bottom-up eDPD model, a top-down particle-based model for mesoscopic thermal transport can be derived from macroscopic PDEs governing the conservations of continuity, momentum, and energy. By introducing thermal fluctuations into an SPH discretization of the (deterministic) Navier-Stokes equations, Español and Revenga (2003) developed the SDPD model. The following SPH discretization was used:

$$
\begin{aligned}
m_i \frac{\mathrm{d}^2 \mathbf{r}_i}{\mathrm{d}t^2} = m_i \frac{\mathrm{d}\mathbf{v}_i}{\mathrm{d}t} &= \sum_j \left[\frac{P_i}{d_i^2} + \frac{P_j}{d_j^2} \right] F_{ij} \mathbf{r}_{ij} - \frac{5\eta}{3} \sum_j \frac{F_{ij}}{d_i d_j} \left[\mathbf{v}_{ij} + (\mathbf{v}_{ij} \cdot \mathbf{e}_{ij}) \mathbf{e}_{ij} \right] , \\
T_i \frac{\mathrm{d}S_i}{\mathrm{d}t} &= \frac{5\eta}{6} \sum_j \frac{F_{ij}}{d_i d_j} \left[\mathbf{v}_{ij}^2 + (\mathbf{v}_{ij} \cdot \mathbf{e}_{ij})^2 \right] - 2\kappa \sum_j \frac{F_{ij}}{d_i d_j} (T_i - T_j) ,
\end{aligned}
\tag{5}
$$

where P and T are the pressure and temperature given by the local equilibrium assumption. The number density d of the fluid particles is computed as $d_i = \sum_j W(|\mathbf{r}_i - \mathbf{r}_j|)$, where $W(r)$ is a compact bell-shaped smoothing kernel (Monaghan 2005). The geometrical factor F_{ij} is given by $F_{ij} = -\nabla W(r_{ij})/r_{ij}$. The transport coefficients are the shear viscosity η and the thermal conductivity κ. The relationship between pressure and density should be specified via an equation of state. The popular choices in SDPD simulations are $p = c^2 \rho$ and $p = p_0(\rho/\rho_0)^\gamma + b$ (Vázquez-Quesada et al. 2009). The first term in the entropy equation is the viscous heating term that captures the physical mechanism by which the energy dissipated by viscous forces transforms into the internal energy. The last term is the heat conduction term induced by the temperature difference between particles.

Using the GENERIC (General Equation for Non-Equilibrium Reversible-Irreversible Coupling) formalism (Grmela and Öttinger 1997; Öttinger and Grmela 1997), thermal fluctuations are then systematically introduced to satisfy the first and second laws of thermodynamics. The velocity and entropy random terms are given by (Español and Revenga 2003)

$$
\begin{aligned}
m_i \mathrm{d}\tilde{\mathbf{v}}_i &= \sum_j A_{ij} \mathrm{d}\hat{\mathbf{W}}_{ij} \cdot \mathbf{e}_{ij} , \\
T_i \mathrm{d}\tilde{S}_i &= -\frac{1}{2} \sum_j A_{ij} \mathrm{d}\hat{\mathbf{W}}_{ij} : \mathbf{e}_{ij} \mathbf{v}_{ij} + \sum_j C_{ij} \mathrm{d}W_{ij}^H ,
\end{aligned}
\tag{6}
$$

respectively, where $\mathrm{d}\hat{\mathbf{W}}_{ij} = (\mathrm{d}\mathbf{W}_{ij} + \mathrm{d}\mathbf{W}_{ij}^T)/2$ is the symmetric part of a matrix of independent increments of the Wiener process $\mathrm{d}\mathbf{W}_{ij}$. $\mathrm{d}W_{ij}^H$ is an independent increment of the Wiener process for each pair of particles, giving rise to the heat conduction terms. Using the fluctuation-dissipation theorem, the parameters A_{ij} and C_{ij} are related to viscosity η and thermal conductivity κ as

$$
A_{ij} = \left[\frac{40}{3} \eta k_B \frac{T_i T_j}{T_i + T_j} \frac{F_{ij}}{d_i d_j} \right]^{1/2} , \quad C_{ij} = \left[4\kappa k_B T_i T_j \frac{F_{ij}}{d_i d_j} \right]^{1/2} . \tag{7}
$$

Thus, the equations of an SDPD model are obtained by adding the stochastic terms in Eq. (6) to the SPH equations in Eq. (5). Kordilla et al. (2014) derived similar stochastic equations by directly discretizing the fluctuating hydrodynamics equations (Ortiz de Zárate and Sengers 2006) with the SPH method.

Although derived using different approaches, the “bottom-up” eDPD and “top-down” SDPD methods have many similarities. Both SDPD and eDPD momentum equations have a conservative force that comes from the gradient of potential energy, a dissipative force induced by viscous friction, and a stochastic term representing thermal fluctuations. SDPD and eDPD energy equations include a heat conduction term to reduce temperature differences between neighboring fluid particles, a viscous heating term to account for the internal energy generated by the viscous dissipation, and a stochastic term induced by thermal fluctuations. In each method, the stochastic contributions in velocities and energies directly relate to the dissipative terms via the fluctuation-dissipation theorem.

Because eDPD was derived from coarse-graining microscopic dynamics (Español et al. 2016), phenomenological expressions for the particle interactions in Eq. (1) can be easily derived to account for complex physics. In the last decade, the bottom-up eDPD approach has been successfully applied to diverse problems involving non-isothermal processes. For example, Cao et al. (2013) used eDPD to simulate natural convection in an eccentric annulus and investigated the effects of various factors on the streamlines and temperature distributions (shown in Fig. 1a). Tang et al. (2016) applied the eDPD method to modeling thermosensitive polymers and simulated the thermally induced self-assembly process of thermoresponsive micelles and vesicles (Fig. 1b). Other examples include heat-stiffening polymer nanocomposites (Cudjoe et al. 2017), thermophoretic microswimmers (Fedosov et al. 2015), natural convection in microchannels (Abu-Nada 2010), and thermoresponsive microgels (Li et al. 2015a).

Due to the similar form of the equations, it should be possible to include complex physics in SDPD using the eDPD coarse-graining procedure. To date, most SDPD applications are concerned with complex fluids and colloidal suspensions (Litvinov et al. 2008; Bian et al. 2012; Lei et al. 2016). The advantage of SDPD for such applications is that the properties of each fluid component, including density, viscosity, and speed of sound, are prescribed directly as model parameters and do not need to be estimated from other model parameters as with eDPD.

3 Mesoscopic Diffusive and Reactive Transport

Many biological processes depend on the concentrations of specific proteins, ions, or other biochemical factors (Anand et al. 2003). For example, proteins in an aqueous solution diffuse in a living cell due to Brownian motion and some collisions of appropriate proteins may lead to chemical reactions. Thus, diffusion and reaction are two fundamental transport processes in biological systems.

For modeling mesoscopic diffusive and reactive transport, Li et al. (2015b) developed a transport dissipative particle dynamics (tDPD) model by defining concentration carried by each DPD particle in addition to other quantities, such as position and momentum. The time evolution of the position and solute concentration of a tDPD particle i with unit mass $m_i \equiv 1$ is governed by the mass and momentum conservation laws, which can be described by the following set of equations:

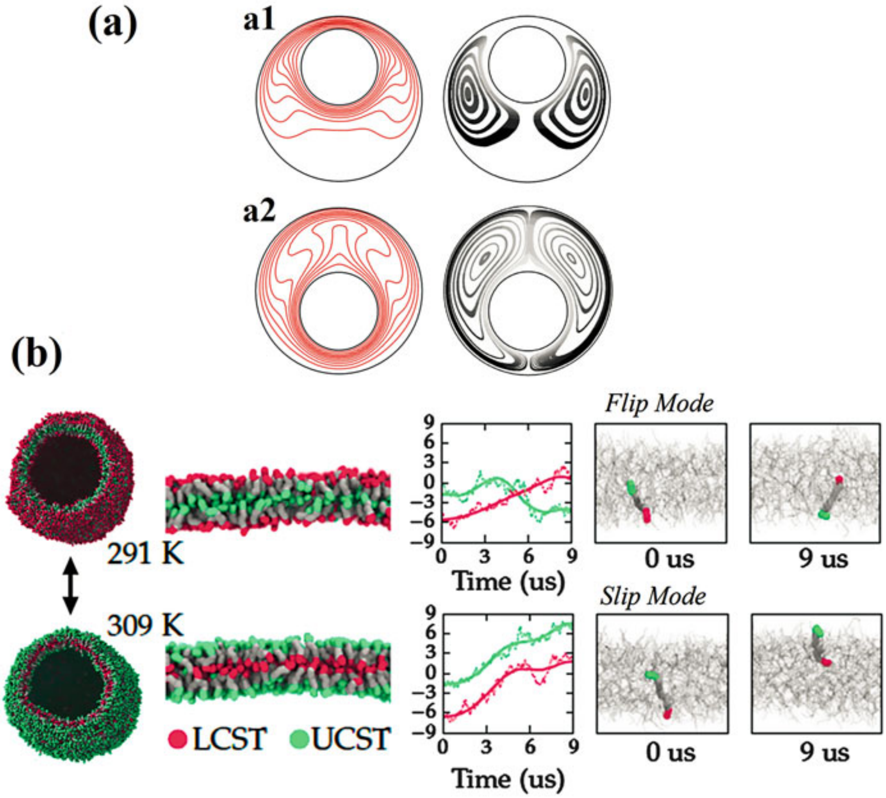

Fig. 1 (**a**) Thermal (left) and flow (right) fields of the natural convection in an eccentric annulus with two different eccentricities. (Adapted from Cao et al. 2013). (**b**) Thermally induced inversion of a unilamellar vesicle formed by triblock copolymers and a proper orthogonal decomposition (POD) analysis showing two dominant molecular movement modes, i.e., flip and slip, during membrane inversion. (Adapted from Tang et al. 2016)

$$\begin{aligned}
\frac{\mathrm{d}^2\mathbf{r}_i}{\mathrm{d}t^2} &= \frac{\mathrm{d}\mathbf{v}_i}{\mathrm{d}t} = \mathbf{F}_i = \sum_{i\neq j}(\mathbf{F}_{ij}^C + \mathbf{F}_{ij}^D + \mathbf{F}_{ij}^R) + \mathbf{F}_i^{\mathrm{ext}}\ , \\
\frac{\mathrm{d}C_i}{\mathrm{d}t} &= Q_i = \sum_{i\neq j}(Q_{ij}^D + Q_{ij}^R) + Q_i^S\ ,
\end{aligned} \tag{8}$$

where t, $\mathbf{r}_i$, $\mathbf{v}_i$, and $\mathbf{F}_i$ denote time and position, velocity, and force vectors, respectively. $\mathbf{F}_i^{\mathrm{ext}}$ is the force on particle i from an external force field. Just as in the classical DPD model, the pairwise interaction between tDPD particles i and j consists of the conservative force $\mathbf{F}_{ij}^C = a_{ij}w_C(r_{ij})\mathbf{e}_{ij}$, dissipative force $\mathbf{F}_{ij}^D = -\gamma_{ij}w_D(r_{ij})(\mathbf{e}_{ij}\cdot\mathbf{v}_{ij})\mathbf{e}_{ij}$, and random force $\mathbf{F}_{ij}^R\mathrm{d}t = \sigma_{ij}w_R(r_{ij})\mathrm{d}W_{ij}\mathbf{e}_{ij}$. C_i represents the concentration of one species defined as the number of a chemical species carried by a tDPD particle i and Q_i, the corresponding concentration flux. The net concentration flux on a particle i accounts for the Fickian flux Q_{ij}^D, the random flux Q_{ij}^R, and a source term Q_{ij}^S generated by local chemical reactions. Because tDPD particles have unit mass, this definition of concentration is equivalent to the concentration in terms of chemical species per unit mass. Then, the volume concentration, i.e., chemical species per unit volume, is ρC_i, where ρ is the number density of tDPD particles. Of note, C_i can be a vector $\mathbf{C}_i$ containing N components, i.e., $\{C_1, C_2, \ldots, C_N\}_i$, when N chemical species are considered.

The driving force for diffusion of each species is the gradient of chemical potential $Q = -DC\nabla\mu/RT$, where D is the diffusion coefficient, R the universal gas constant, T the absolute temperature, and μ the chemical potential given by $\mu = \mu_0 + RT \ln C$ for dilute solutions (Ortiz de Zárate and Sengers 2006). By substituting the chemical potential μ into the expression for Q, the diffusion driving force is found to be proportional to the concentration gradient ∇C, which corresponds to a concentration difference between two neighboring tDPD particles. It follows that the Fickian and random fluxes in the tDPD model are given by

$$Q_{ij}^D = -\kappa_{ij} w_{DC}(r_{ij}) \left(C_i - C_j\right) , \quad Q_{ij}^R \mathrm{d}t = \varepsilon_{ij} w_{RC}(r_{ij}) \mathrm{d}W_{ij}^{cc} , \tag{9}$$

where κ_{ij} and ε_{ij} determine the strength of the Fickian and random fluxes. $\mathrm{d}W_{ij}^{cc} = \mathrm{d}W_{ji}^{cc}$ are independent increments of the Wiener process. $w_{DC}(r)$ and $w_{RC}(r)$ are weight functions with a cutoff radius r_{cc}. The Fickian friction parameter κ plays the analogous role for concentration differences between tDPD particles, as γ does for momentum. In general, the concentration friction κ is a $N \times N$ matrix when the interdiffusivities of N different chemical species are involved. However, considering N chemical species in dilute solution and neglecting the interdiffusivities of different species, the system is then reduced to a set of uncoupled diffusion equations with independent diffusivities between species. Hence, κ becomes a diagonal matrix (Balluffi et al. 2005).

By applying the local-equilibrium assumption to the tDPD system, the random term Q_{ij}^R is related to the dissipative term Q_{ij}^D by satisfying the fluctuation-dissipation theorem (Li et al. 2015b)

$$\varepsilon_{ij}^2 = m_s^2 \kappa_{ij} \rho (C_i + C_j) , \quad w_{DC}(r_{ij}) = w_{RC}^2(r_{ij}) , \tag{10}$$

where m_s is the mass of a single solute molecule, while C_i and C_j are the respective concentrations on particles i and j. For detailed derivations for obtaining Eq. (10), refer to Li et al. (2015b). In general, the mass of a single solute molecule m_s is much smaller than that of a tDPD particle m, which is often chosen as the mass unit. Consequently, the magnitude of ε is small for $m_s \ll m$, which indicates that the contribution of the random flux Q_{ij}^R to the total diffusion coefficient D is negligible unless m_s becomes comparable to m in nanoscale systems.

The macroscopic properties, including viscosity and diffusivity of a tDPD system, are output properties rather than input parameters. Due to the random movements of tDPD particles generated by stochastic forces, the effective diffusion coefficient D consists of both the random diffusion D^ξ and the Fickian diffusion D^F. In general, the random contribution D^ξ is a combined result of the random movements of tDPD particles and random flux Q_{ij}^R in Eq. (9). However, the variance of random flux Q_{ij}^R has a small prefactor m_s^2 as given by Eq. (10). Thus, the contribution of the random flux Q_{ij}^R to D^ξ is negligible in practical applications. In the derivations, it is assumed that D^ξ is induced by the random movements of tDPD particles. In particular, for a tDPD system in thermal equilibrium, the diffusion coefficient D^ξ induced by the random movements of tDPD particles and the macroscopic diffusion coefficient D^F due to the Fickian flux can be calculated by Li et al. (2015b)

$$D^\xi = \frac{3k_B T}{4\pi\gamma\rho \cdot \int_0^{r_c} r^2 w_D(r) g(r) dr}\ , \quad D^F = \frac{2\pi\kappa\rho}{3}\int_0^{r_{cc}} r^4 w_{DC}(r) g(r) dr\ , \tag{11}$$

where r_c is the cutoff radius for forces and r_{cc} is the cutoff radius for concentration flux. Let $w_D(r) = (1 - r/r_c)^{s_1}$ and $w_{DC}(r) = (1 - r/r_{cc})^{s_2}$ be the weight functions of the dissipative force $\mathbf{F}_{ij}^D$ and the Fickian flux Q_{ij}^D, respectively. When the radial distribution function of ideal gas $g(r) = 1.0$ is employed, both D^ξ and D^F can be evaluated analytically as $D = D^\xi + D^F = 3k_B T \prod_{i=1}^3 (s_1 + i)/8\pi\gamma\rho r_c^3 + 16\pi\kappa\rho r_{cc}^5/\prod_{i=1}^5 (s_2 + i)$, where s_1 and s_2 are the exponents of $w_D(r)$ and $w_{DC}(r)$.

Because the particle-based tDPD method satisfies the conservation of concentration automatically, it provides an economical way to solve advection-diffusion-reaction (ADR) equations with a large number of species. Xu et al. (2011) used a two-dimensional model to investigate biofilm growth in a narrow channel and demonstrated the effects of flow velocity, growth parameter, and hydrodynamic interaction on the biofilm growth regime and morphology. Li et al. (2015b) employed tDPD to study the dynamic process of blood coagulation, modeled by a set of 23 coupled ADR equations for the evolution of 25 biological reactants involved in a combined model of intrinsic and extrinsic pathways of blood coagulation process and fibrinolysis. They reported the tDPD simulation correctly produced the thrombin burst followed by a drop and provided qualitatively correct evolution of fibrin concentration initialized by an injured vessel wall in flowing blood (shown in Fig. 2a).

Alternatively, mesoscopic mass transport can be modeled by a top-down approach: numerically solving the fluctuating hydrodynamics equations, including the continuity equation $\mathrm{d}\rho/\mathrm{d}t = -\rho(\nabla \cdot \mathbf{v})$ and momentum conservation equation $\rho\mathrm{d}\mathbf{v}/\mathrm{d}t = -\nabla P + \nabla \cdot \tau + \nabla \cdot \mathbf{s}$ with a random stress tensor $\mathbf{s}$ and the stochastic advection-diffusion equation $\rho\mathrm{d}C/\mathrm{d}t = \nabla \cdot (D\nabla C) + \nabla \cdot \mathbf{J}$ with a random flux vector $\mathbf{J}$ (Ortiz de Zárate and Sengers 2006). Using the fluctuation-dissipation theorem, the random stress in the momentum equation is related to the viscous stress, while the random concentration flux in the advection-diffusion equation relates to the Fickian diffusion. Kordilla et al. (2014) used SPH discretization to solve these equations. Similar to the tDPD model, the effective diffusion coefficient D in the SPH-based model (Kordilla et al. 2014) consists of a deterministic Fickian coefficient D^F and stochastic contribution D^ξ.

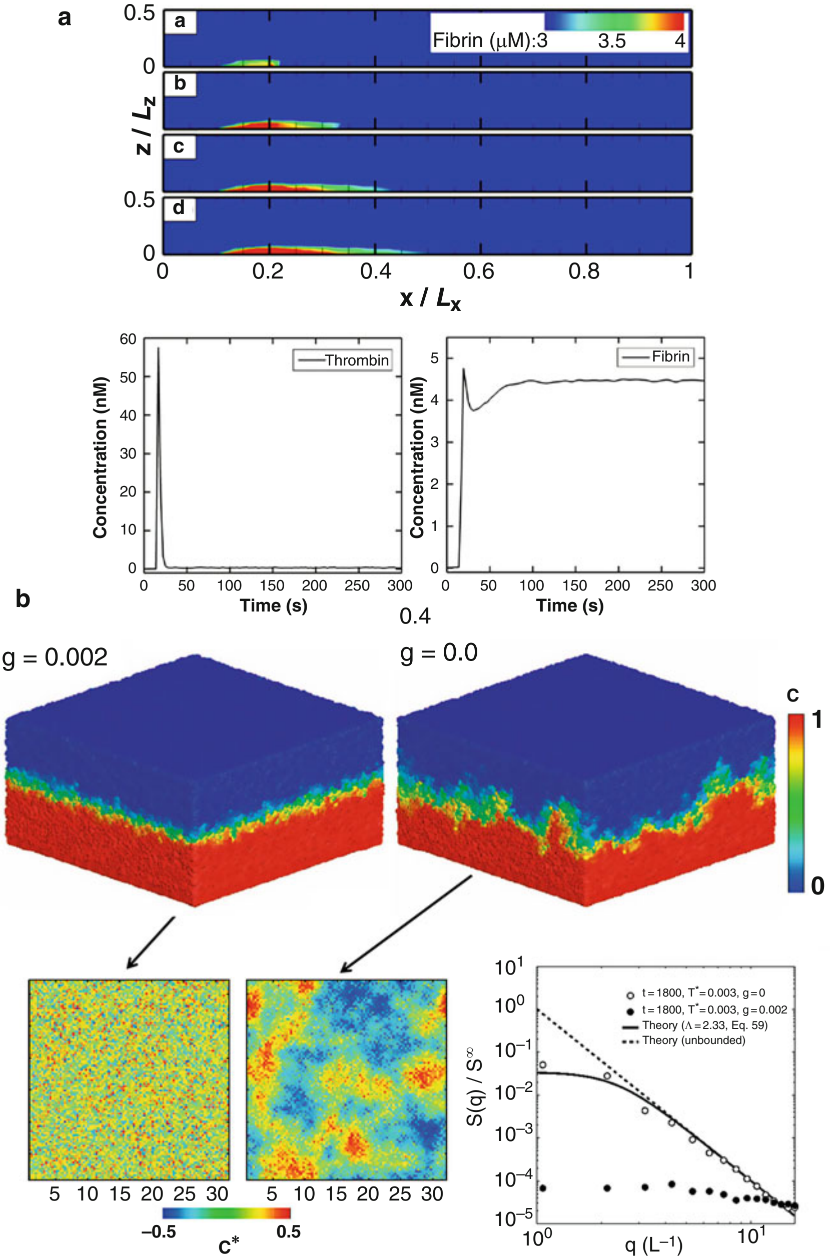

Fig. 2 (**a**) Time evolution of the fibrin concentration field during the dynamic process of blood coagulation in flowing blood and the concentrations of thrombin and fibrin at the center of the injured wall region. (Adapted from Li et al. 2015b). (**b**) Formation of "giant fluctuations" of the front between light and heavy fluids with and without gravity, where the light fluid is on the top of the heavy fluid. The map shows the concentration field, and the plot shows corresponding power spectra of the concentration field. (Adapted from Kordilla et al. 2014)

Kordilla et al. (2014) applied this SPH-based model for studying the formation of “giant fluctuations” of the front between light and heavy fluids with and without gravity, where the light fluid is on top of the heavy fluid (shown in Fig. 2b). Their results indicate that the presence of gravity significantly reduces front perturbations for all considered values of Fickian diffusion D_F, but the effect of gravity becomes less pronounced as D^F increases. When the Fickian diffusion D_F becomes significantly larger than D_ξ, the stochastic diffusion reduces to a deterministic diffusion, and fluctuations completely disappear. Kordilla et al. (2014) also demonstrated that in the absence of gravity, the SPH-based model recovers the characteristic q^-4 divergence of the interface power spectrum and its scale-invariant nature, which are in good agreement with the experiments and analytical solutions.

4 Mesoscopic Ionic Transport

Ionic transport is ubiquitous in biological processes and is extremely important in the vital activity of all organisms. The concentration gradient of potassium ion K^+, sodium ion Na^+, and calcium ion Ca^{2+} across the cell membrane is the basis for the transmission of excitation in organisms. It is not surprising that ionic transport is implicated in numerous diseases. For example, cystic fibrosis is an autosomal recessive disease, which is induced by defective ion transport and characterized by hyperabsorption of Na^+ in the airway epithelia (Kunzelmann and Mall 2003). Transport of Ca^{2+} from muscle cells leads to relaxation of muscles, while the entry of these ions into the cytoplasm upon excitation produces muscle contraction (Rüegg 1992). An inherited skeletal muscle disorder, named Brody disease, is clinically characterized by exercise-induced muscle stiffness, rooted from abnormal Ca^{2+} transport (Guglielmi et al. 2013). Also, the flux of ions across the membranes of neurons changes the electrochemical gradient and results in the production of an electrical signal sent between neurons in the brain (Purves et al. 2004). Disruption of ionic homeostasis significantly affects the neuron activities. Alzheimer’s disease is associated with increased intracellular Na^+ and K^+ levels in brain regions, which is induced by imbalanced ionic transport contributed to the pathophysiology of Alzheimer’s disease (Vitvitsky et al. 2012). Understanding the functional role and mechanism of ionic transport at cellular/subcellular levels is of crucial physiological importance to develop new diagnostic tests for diseases and to discover novel drug molecules (Modi et al. 2012).

However, simulating fluctuating electrohydrodynamic phenomena with fully coupled hydrodynamics and electrostatics with long-range Coulomb interactions is challenging. Here, a variant of DPD method is used to tackle this challenge. It extends the classical DPD method that has proven accurate and effective in modeling mesoscopic fluctuating hydrodynamics (Groot and Warren 1997) and introduces ions represented by explicit charged particles in a DPD system. The electrostatic interactions between these ions can be computed by two approaches: (1) all interactions between the charged particles are summed in real space, and (2) all charged particles are projected onto a local electrostatic field that is governed by the Poisson's equation $\nabla(\varepsilon \nabla \varphi) = -\beta e^2 \rho$ and solved separately.

As a consequence of the soft interactions in the DPD model, charged particles may overlap and form infinitely strongly bound ion pairs through electrostatic interactions. To avoid overlapping of charged DPD particles, Groot (2003) distributed the charge within an electrostatic smearing radius R_e using a charge distribution $f(r) = 3(1 - r/R_e)/\pi R_e^3$, while González-Melchor et al. (2006) used a Slater-type charge distribution $f(r) = \exp(-2r/\lambda)/\pi\lambda^3$ with a decay length λ. With explicit ions, the Ewald summation method (Ewald 1921) is a widely used route to calculate electrostatic interactions in particle systems. Because point charges interact according to Coulomb's law, the total electrostatic energy for a periodic cubic system of side L is given by

$$U(\mathbf{r}) = \frac{1}{4\pi\varepsilon_0\varepsilon_r} \sum_{i} \sum_{j>i} \sum_{\mathbf{r}} \frac{q_i q_j}{|\mathbf{r}_{ij} + \mathbf{n}L|}, \tag{12}$$

where $\mathbf{n} = (n_x, n_y, n_z)$ with n_x, n_y, and n_z being integer numbers. The sum over $\mathbf{n}$ takes into account the periodic images. The Ewald treatment decomposes the long-range electrostatic energy in a real space and the reciprocal space contributions, so both the real and reciprocal parts can be computed by short-ranged sums as an approach to $1/r$, capturing the full long-range nature of electrostatic interactions (González-Melchor et al. 2006).

Different from a direct calculation of the electrostatic forces, Groot (2003) introduced a lattice to the DPD system and spread out the charges over the lattice nodes. Then, the long-range portion of the interaction potential was calculated by solving the Poisson equation on the grid based on a particle-particle particle-mesh (PPPM) algorithm by transferring quantities (charges and forces) from the particles to the mesh and vice versa. It has been noted that the PPPM method works efficiently in DPD if the grid size equals the particle size. Because the mesh defines a coarse-graining length for electrostatic interactions, correlation effects on length scales shorter than the mesh size cannot be properly accounted for. Explicit treatment of the ions is computationally expensive, especially for systems with high ionic concentrations. To this end, Medina et al. (2015) developed a Condiff-DPD model with ions represented by the concentration of the ionic species. They used DPD equations for fluid particles and Brownian pseudo particles to describe the evolution of the ionic concentrations. Instead of direct interactions, the pseudo-ions and DPD particles are coupled through a lattice, where the Poisson equation is solved using the PPPM algorithm. Compared to "explicit-ion" simulations whose computational costs depend on the number of ions, the cost for electrostatic calculations in a simulation with "implicit ions" is dominated by the cost for solving the Poisson equation. Using the PPPM method, the cost primarily depends on the number of mesh points.

Although, the particle-to-mesh and then mesh-to-particle mapping/redistribution can solve the Poisson equation for particle-based systems (Groot 2003), its dependence on a grid may contradict the original motivation for using a Lagrangian method, and additional computational complexity and inefficiencies are introduced. To abandon grids and use a unifying Lagrangian description for mesoscopic electrokinetic phenomena, Deng et al. (2016) developed a charged DPD, or cDPD, model, where the Poisson equation is solved on moving cDPD particles rather than grids. Specifically, cDPD describes the solvent explicitly in a coarse-graining sense as DPD particles, while the ion species are described semi-implicitly, i.e., using a Lagrangian description of ionic concentration fields, associated with each moving cDPD particle, which provides a natural coupling between fluctuating electrostatics and hydrodynamics.

The state vector of a cDPD particle can be written as $(\mathbf{r}, \mathbf{v}, c_\alpha, \phi)$, which is not only characterized by its position $\mathbf{r}$ and velocity $\mathbf{v}$ as in the classical DPD model but also by ionic species concentration c_α (with α representing the αth ion type) and electrostatic potential ϕ on the particle. A cDPD particle is then viewed as a coarse-grained fluid volume, which contains the solvent and other charged species. Exchange of the concentration flux of charged species occurs between neighboring cDPD particles, much like the momentum exchange in the classical DPD model. The time evolution of the state vector of a cDPD particle i with unit mass $m_i \equiv 1$ is governed by the following set of stochastic differential equations:

$$\begin{aligned} \frac{d^2\mathbf{r}_i}{dt^2} &= \frac{d\mathbf{v}_i}{dt} = \mathbf{F}_i = \sum_{i\neq j}(\mathbf{F}_{ij}^C + \mathbf{F}_{ij}^D + \mathbf{F}_{ij}^R + \mathbf{F}_{ij}^E), \\ \frac{dc_{\alpha i}}{dt} &= q_{\alpha i} = \sum_{i\neq j}(q_{\alpha ij}^D + q_{\alpha ij}^E + q_{\alpha ij}^R), \end{aligned} \tag{13}$$

where the total force $\mathbf{F}_i$ consists of three pairwise forces as in classical DPD method, i.e., the conservative force $\mathbf{F}_{ij}^C = a_{ij} w_C(r_{ij})\mathbf{e}_{ij}$, dissipative force $\mathbf{F}_{ij}^D = -\gamma_{ij} w_D(r_{ij})(\mathbf{e}_{ij} \cdot \mathbf{v}_{ij})\mathbf{e}_{ij}$, and random force $\mathbf{F}_{ij}^R = \sigma_{ij} w_R(r_{ij})\xi_{ij}\mathbf{e}_{ij}$, as well as an electrostatic force $\mathbf{F}^E$ coupling hydrodynamics and electrokinetics, given by

$$\mathbf{F}_{ij}^E = \lambda_{ij}\rho_{ei}\mathbf{E}_{ij}, \quad \mathbf{E}_{ij} = (\phi_i - \phi_j)\omega_E(r_{ij})\hat{\mathbf{r}}_{ij}, \tag{14}$$

where the coupling parameter λ_{ij} is linearly related to the macroscopic dimensionless coupling parameter $\Lambda = c_0 k_B T \tau^2/(\rho_0 r_0^2)$ with c_0 and ρ_0 as the reference concentration and reference mass density, which are chosen as the respective salt concentration and mass density of bulk solution. r_0 and τ are the unit length and time in DPD. $\rho_{ei} = \sum_\alpha z_\alpha c_{\alpha i}$ is the total charge density within the ith particle, and $\mathbf{E}_{ij}$ is the relative electric field determined by the difference of electrostatic potential field between particles i and j and a weighting function $\omega_E(r)$. Although the electrostatic forces are essentially not pairwise, i.e., $\mathbf{F}_{ij}^E \neq \mathbf{F}_{ji}^E$, a zero total force condition $\sum_{i,j}\mathbf{F}_{ij}^E = 0$ is always satisfied because of the charge neutrality condition $\sum_i\sum_\alpha z_\alpha c_{\alpha i} = 0$, which guarantees the global momentum conservation if there is no external electrostatic field.

Transport equations of ionic species are implemented in the cDPD model by introducing extra degrees of freedom and corresponding evolution equations associated with each cDPD particle. Diffusion of ionic species is driven by three flux terms, i.e., the Fickian flux q_{ij}^D induced by the concentration gradient, electrostatic flux q_{ij}^E induced by electrostatic potential gradient, and random flux q_{ij}^R due to thermal fluctuations, which can be written as

$$\begin{aligned} q_{\alpha ij}^D &= -\kappa_{\alpha ij}\ (c_{\alpha i} - c_{\alpha j})\ \omega_{qD}(r_{ij}), \\ q_{\alpha ij}^E &= -\kappa_{\alpha ij}\ z_\alpha\ \overline{c}_{\alpha ij}\ (\phi_i - \phi_j)\ \omega_{qD}(r_{ij}), \\ q_{\alpha ij}^R &= \xi_{\alpha ij}\ \omega_{qR}(r_{ij})\ \theta_{ij}\ \delta t^{-1/2}, \end{aligned} \tag{15}$$

where $\overline{c}_{\alpha ij} = (c_{\alpha i} + c_{\alpha j})/2$ is the average ionic concentration, $\kappa_{\alpha ij}$ is the diffusion coefficients of the αth species, and $\omega_{qD}(r_{ij})$ is a weighting function. The parameters in q_{ij}^D and q_{ij}^R are related via the generalized fluctuation-dissipation theorem, i.e., $\omega_{qD}(r) = \omega_{qR}^2(r)$ and $\xi_{\alpha ij}^2 = \kappa_{\alpha ij}(c_{\alpha i} + c_{\alpha j})/c_0 r_0^3$, which suggests that the variance of random flux is proportional to r_0^{-3}. Thus, the random flux cannot be neglected in micro-/nanoscales where $r_0 \ll 10^{-6}m$.

The electrostatic potential ϕ on each cDPD particle is determined by solving the Poisson equation at every time step. Consider the dimensionless Poisson equation rescaled by the DPD units $\nabla(\varepsilon(\mathbf{r})\nabla\phi(\mathbf{r})) = -\Gamma\rho_e(\mathbf{r})$, where $\varepsilon(\mathbf{r})$ is the local relative permittivity and $\Gamma = e^2 c_0 r_0^2/\varepsilon_0 k_B T$. The Poisson equation should be solved at every time step using, for example, a successive over-relaxation iteration scheme. Then, the electrostatic potential ϕ_i on the ith cDPD particle is obtained iteratively as

$$\phi_i^k = \phi_i^{k-1} + \vartheta\left[\chi\rho_{ei} - \sum_{j\neq i}\overline{\varepsilon}_{ij}\phi_{ij}^k\omega_\phi(r_{ij})\right], \tag{16}$$

where χ is linearly related to the macroscopic parameter Γ that characterizes the strength of the electrostatic interactions, $\overline{\varepsilon}_{ij} = (\varepsilon_i + \varepsilon_j)/2$ is the average permittivity, $\omega_\phi(r)$ is a weight function, and ϑ is a relaxation factor. The value of ϑ can be adaptively changed during the iteration process, and the value of ϕ_i at the previous time step can be taken as an initial estimate of ϕ_i^{k-1} to achieve faster convergence. Then, the iteration of Eq. (16) is performed until the absolute differences $|\phi_i^k - \phi_i^{k-1}|$ are below a predefined tolerance.

Both the DPD model based on explicit ions (Groot 2003) and the cDPD model based on semi-implicit ions (Deng et al. 2016) have been applied to fluctuating electrohydrodynamic phenomena investigations. Posel et al. (2014) applied Groot's DPD model with explicit ions (Groot 2003) to study pH-dependent self-assembly of poly(2-vinylpyridine)-block-poly(ethylene oxide) diblock copolymers in aqueous media. They quantified the dependences of the apparent radius of gyration and

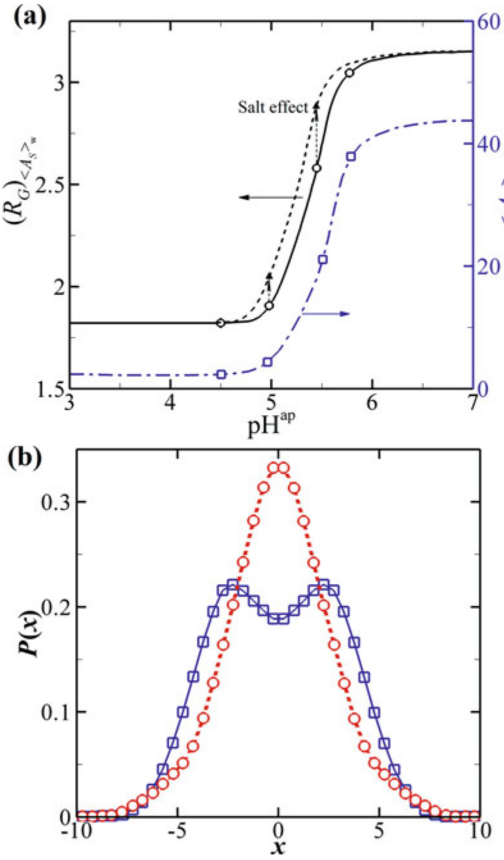

Fig. 3 (**a**) Apparent radius of gyration $(R_G)_{\langle A_S \rangle_w}$ and weight-averaged association number $\langle A_S \rangle_w$ as functions of the pH^{ap}, where the effect of the salt is depicted by the shift in the radius of gyration. (Adapted from Posel et al. 2014). (**b**) Mass density distribution for both positive (blue squares)- and negative (red circles)-charged polyelectrolytes drifting in electroosmotic flow between two positively charged surfaces. (Adapted from Deng et al. 2016)

weight-averaged association number on pH, shown in Fig. 3a, and simulated the micellization process that coincides credibly with experimental observations. Deng et al. (2016) used the cDPD model to simulate the dilute polyelectrolyte solution drifting by electroosmotic flow in a microchannel. Unlike the migration of an uncharged polymer in the channel flow, they reported that negative-charged polyelectrolytes are likely to remain at the channel center because of the electrostatic repulsion from the charged surface, while the positive-charged polyelectrolytes drift away from the center with double peaks (Fig. 3b). Moreover, Zhou et al. (2013) investigated the response of a charged colloid and its surrounding microion cloud to an alternating electric field. Moshfegh and Jabbarzadeh (2016) simulated the electroosmotic flow in narrow nanochannels via explicit electrostatic interactions computed using the Ewald summation method. The authors acknowledge they currently are not aware of any top-down mesoscopic particle-based methods for ionic transport that consistently incorporate thermal fluctuations.

5 Summary

This chapter has considered different particle-based methods for mesoscopic transport processes, including thermal transport, reactive biochemical transport, and ionic transport in mesoscopic systems. These mesoscopic methods consistently incorporate thermal fluctuations based on non-equilibrium thermodynamics and are capable of describing certain mesoscopic features that deterministic macroscopic methods cannot model. The equations of a particle-based mesoscopic model can be derived from either bottom-up coarse-graining of microscopic dynamics or top-down discretization of macroscopic PDEs. Regardless of how mesoscopic models are obtained, they have similar structures, representing relevant physical mechanisms that dominate mesoscopic processes. Because mesoscopic methods are grounded in both macroscale and micro-/nanoscale models, they can play an important role in multiscale modeling of diseases and relevant bioengineering applications by seamlessly bridging the gap between microscopic molecular biology and macroscopic bulk behavior.

Despite considerable developments in recent years, particle-based mesoscopic methods are still evolving. New variations in models, novel theoretical interpretations, and innovative numerical algorithms often appear in literature. These methods have been applied to a large number of problems, including polymer and colloidal suspensions, multiphase fluids, biological materials, cell dynamics, and blood rheology, and new applications in different areas are still emerging. In the near future, these methods likely will be used even more widely for tackling challenging problems in biorheology, cellular biology, and bioengineering.

Additional research is needed in several areas, including the parameterization of mesoscopic models. Tuning model parameters manually by trial and error only works for simple systems. For problems with high-dimensional parameter spaces, Bayesian and/or machine-learning methods hold significant promise for inferring the model parameters (Lei et al. 2017). Coupling mesoscopic methods with other micro-/macroscopic methods to handle multiscale problems is another emerging research area. With concurrent coupling algorithms, i.e., domain decomposition (Tang et al. 2015) or adaptive resolution scheme (Praprotnik et al. 2006), in the lower limits, the mesoscopic methods can be coupled with microscale techniques, while in the upper bounds, the mesoscopic methods can be coupled with discretized PDEs. However, in concurrently coupled system, preserving correct fluctuations across the interface of heterogeneous solvers remains a challenging problem. Moreover, there is a need to decrease the computational cost of mesoscale methods, which could be achieved, for example, by improving the integration algorithms (Leimkuhler and Shang 2015) and efficient parallel implementations with graphics processing units (Blumers et al. 2017). Domain decomposition is routinely used to improve the scalability of particle codes. Parallel-in-time algorithms should be also investigated to further increase mesoscale method performance.

Acknowledgments This work was supported by the US Army Research Laboratory under Cooperative Agreement No. W911NF-12-2-0023. A. M. Tartakovsky was supported by the US Department of Energy (DOE), Office of Science, Office of Advanced Scientific Computing Research at Pacific Northwest National Laboratory (PNNL). PNNL is operated by Battelle for the DOE under Contract DE-AC05-76RL01830. The authors thank Charity Plata for a very thorough reading of the manuscript.

References

Abu-Nada E (2010) Natural convection heat transfer simulation using energy conservative dissipative particle dynamics. Phys Rev E 81(5):056704

Anand M, Rajagopal K, Rajagopal KR (2003) A model incorporating some of the mechanical and biochemical factors underlying clot formation and dissolution in flowing blood. J Theor Med 5(3-4):183–218

Avalos JB, Mackie AD (1997) Dissipative particle dynamics with energy conservation. Europhys Lett 40(2):141–146

Balluffi RW, Allen SM, Carter WC (2005) Kinetics of materials. Wiley, Hoboken

Bian X, Litvinov S, Qian R, Ellero M, Adams NA (2012) Multiscale modeling of particle in suspension with smoothed dissipative particle dynamics. Phys Fluids 24(1):012002

Blumers AL, Tang YH, Li Z, Li X, Karniadakis GE (2017) GPU-accelerated red blood cells simulations with transport dissipative particle dynamics. Comput Phys Commun 217:171–179

Cao ZH, Luo K, Yi HL, Tan HP (2013) Energy conservative dissipative particle dynamics simulation of natural convection in eccentric annulus. Int J Heat Mass Trans 65:409–422

Chen M, Li F, Wang S, Cao Y (2017) Stochastic modeling and simulation of reaction-diffusion system with Hill function dynamics. BMC Syst Biol 11:21

Cudjoe E, Khani S, Way AE, Hore MJA, Maia J, Rowan SJ (2017) Biomimetic reversible heat-stiffening polymer nanocomposites. ACS Cent Sci 3(8):886–894

Deng M, Li Z, Borodin O, Karniadakis GE (2016) cDPD: a new dissipative particle dynamics method for modeling electrokinetic phenomena at the mesoscale. J Chem Phys 145:144109

Drawert B, Hellander S, Trogdon M, Yi TM, Petzold L (2016) A framework for discrete stochastic simulation on 3D moving boundary domains. J Chem Phys 145(18):184113

Español P (1997) Dissipative particle dynamics with energy conservation. Europhys Lett 40(6):631–636

Español P, Revenga M (2003) Smoothed dissipative particle dynamics. Phys Rev E 67:026705

Español P, Warren P (1995) Statistical mechanics of dissipative particle dynamics. Europhys Lett 30(4):191–196

Español P, Serrano M, Pagonabarraga I, Zúñiga I (2016) Energy-conserving coarse-graining of complex molecules. Soft Matter 12(21):4821–4837

Ewald PP (1921) Die berechnung optischer und elektrostatischer gitterpotentiale. Ann Phys 369(3):253–287

Fedosov DA, Sengupta A, Gompper G (2015) Effect of fluid-colloid interactions on the mobility of a thermophoretic microswimmer in non-ideal fluids. Soft Matter 11(33):6703–6715

González-Melchor M, Mayoral E, Velázquez ME, Alejandreb J (2006) Electrostatic interactions in dissipative particle dynamics using the Ewald sums. J Chem Phys 125:224107

Grmela M, Öttinger HC (1997) Dynamics and thermodynamics of complex fluids. I. Development of a general formalism. Phys Rev E 56(6):6620–6632

Groot RD (2003) Electrostatic interactions in dissipative particle dynamics-simulation of polyelectrolytes and anionic surfactants. J Chem Phys 118(24):11265–11277

Groot RD, Warren PB (1997) Dissipative particle dynamics: bridging the gap between atomistic and mesoscopic simulation. J Chem Phys 107(11):4423–4435

Guglielmi V, Voermans NC, Gualandi F, Van Engelen BG, Ferlini A, Tomelleri G, Vattemi G (2013) Fourty-four years of brody disease: it is time to review. J Genet Syndr Gene Ther 4(9):1–8

Hellander A (2008) Efficient computation of transient solutions of the chemical master equation based on uniformization and quasi-Monte Carlo. J Chem Phys 128(15):154109

Kordilla J, Pan W, Tartakovsky A (2014) Smoothed particle hydrodynamics model for Landau-Lifshitz-Navier-Stokes and advection-diffusion equations. J Chem Phys 141:224112

Kunzelmann K, Mall M (2003) Pharmacotherapy of the ion transport defect in cystic fibrosis. Am J Respir Med 2(4):299–309

Lei H, Baker NA, Wu L, Schenter GK, Mundy CJ, Tartakovsky AM (2016) Smoothed dissipative particle dynamics model for mesoscopic multiphase flows in the presence of thermal fluctuations. Phys Rev E 94:023304

Lei H, Yang X, Li Z, Karniadakis GE (2017) Systematic parameter inference in stochastic mesoscopic modeling. J Comput Phys 330:571–593

Leimkuhler B, Shang X (2015) On the numerical treatment of dissipative particle dynamics and related systems. J Comput Phys 280:72–95

Li Z, Tang YH, Lei H, Caswell B, Karniadakis GE (2014) Energy-conserving dissipative particle dynamics with temperature-dependent properties. J Comput Phys 265:113–127

Li Z, Tang YH, Li X, Karniadakis GE (2015a) Mesoscale modeling of phase transition dynamics of thermoresponsive polymers. Chem Commun 51(55):11038–11040

Li Z, Yazdani A, Tartakovsky A, Karniadakis GE (2015b) Transport dissipative particle dynamics model for mesoscopic advection-diffusion-reaction problems. J Chem Phys 143:014101

Li Z, Bian X, Li X, Deng M, Tang YH, Caswell B, Karniadakis GE (2017) Dissipative particle dynamics: foundation, evolution, implementation, and applications. Birkhäuser, Cham, pp 255–326

Litvinov S, Ellero M, Hu X, Adams NA (2008) Smoothed dissipative particle dynamics model for polymer molecules in suspension. Phys Rev E 77:066703

Mackie AD, Avalos JB, Navas V (1999) Dissipative particle dynamics with energy conservation: Modelling of heat flow. Phys Chem Chem Phys 1(9):2039–2049

Marsh CA, Backx G, Ernst MH (1997) Static and dynamic properties of dissipative particle dynamics. Phys Rev E 56(2):1676–1691

Medina S, Zhou J, Wang ZG, Schmid F (2015) An efficient dissipative particle dynamics-based algorithm for simulating electrolyte solutions. J Chem Phys 142(2):024103

Modi N, Winterhalter M, Kleinekathofer U (2012) Computational modeling of ion transport through nanopores. Nanoscale 4(20):6166–6180

Monaghan JJ (2005) Smoothed particle hydrodynamics. Rep Prog Phys 68(8):1703–1759

Moshfegh A, Jabbarzadeh A (2016) Fully explicit dissipative particle dynamics simulation of electroosmotic flow in nanochannels. Microfluid Nanofluid 20(4):67

Ortiz de Zárate JM, Sengers JV (2006) Hydrodynamic fluctuations in fluids and fluid mixtures. Elsevier, Amsterdam

Öttinger HC, Grmela M (1997) Dynamics and thermodynamics of complex fluids. II. Illustrations of a general formalism. Phys Rev E 56(6):6633–6655

Perez-Herrero E, Fernandez-Medarde A (2015) Advanced targeted therapies in cancer: drug nanocarriers, the future of chemotherapy. Eur J Pharm Biopharm 93:52–79

Posel Z, Limpouchova Z, Sindelka K, Lisal M, Prochazka K (2014) Dissipative particle dynamics study of the pH-dependent behavior of poly(2-vinylpyridine)-block-poly(ethylene oxide) diblock copolymer in aqueous buffers. Macromolecules 47(7):2503–2514

Praprotnik M, Delle Site L, Kremer K (2006) Adaptive resolution scheme for efficient hybrid atomistic-mesoscale molecular dynamics simulations of dense liquids. Phys Rev E 73:066701

Purves D, Augustine GJ, Fitzpatrick D, Hall WC, LaMantia AS, McNamara JO, Williams SM (2004) Neuroscience, 3rd edn. Sinauer Associates, Inc., Sunderland, Massachusetts U.S.A.

Rüegg JC (1992) Calcium in muscle contraction: cellular and molecular physiology. 2nd edn. Springer-Verlag Berlin

Schnoerr D, Sanguinetti G, Grima R (2017) Approximation and inference methods for stochastic biochemical kinetics – a tutorial review. J Phys A Math Theor 50(9):1–60

Taghizadeh B, Taranejoo S, Monemian SA, Moghaddam ZS, Daliri K, Derakhshankhah H, Derakhshani Z (2015) Classification of stimuli-responsive polymers as anticancer drug delivery systems. Drug Deliv 22(2):145–155

Tang YH, Kudo S, Bian X, Li Z, Karniadakis GE (2015) Multiscale universal interface: a concurrent framework for coupling heterogeneous solvers. J Comput Phys 297:13–31

Tang YH, Li Z, Li X, Deng M, Karniadakis GE (2016) Non-equilibrium dynamics of vesicles and micelles by self-assembly of block copolymers with double thermoresponsivity. Macromolecules 49(7):2895–2903

Vázquez-Quesada A, Ellero M, Español P (2009) Consistent scaling of thermal fluctuations in smoothed dissipative particle dynamics. J Chem Phys 130:034901

Vitvitsky VM, Garg SK, Keep RF, Albin RL, Banerjee R (2012) Na^+ and K^+ ion imbalances in Alzheimer's disease. Biochim Biophys Acta Mol Basis Dis 1822(11):1671–1681

Xu Z, Meakin P, Tartakovsky A, Scheibe TD (2011) Dissipative-particle-dynamics model of biofilm growth. Phys Rev E 83(6):066702

Zhou J, Schmitz R, Dunweg B, Schmid F (2013) Dynamic and dielectric response of charged colloids in electrolyte solutions to external electric fields. J Chem Phys 139:024901